Unusually long free carrier lifetime and metal-insulator band offset in vanadium dioxide

Chris Miller, Mark Triplett, Joel Lammatao, Joonki Suh, Deyi Fu, Junqiao Wu, and Dong Yu

Phys. Rev. B **85**, 085111 — Published 15 February 2012

DOI: 10.1103/PhysRevB.85.085111

Unusually long free carrier lifetime and metal-insulator band offset in vanadium dioxide

Chris Miller,[1] Mark Triplett,[1] Joel Lammatao,[1] Joonki Suh,[2] Deyi Fu,[2,3] Junqiao Wu,[2] and Dong Yu[*,1]*

[1]Department of Physics, University of California, Davis, CA 95616, USA

[2]Department of Materials Science and Engineering, University of California, Berkeley, CA 94720, USA

[3]Jiangsu Provincial Key Laboratory of Advanced Photonic and Electronic Materials, School of Electronic Science and Engineering, Nanjing University, Nanjing 210093, China

Receipt date (to be automatically inserted after your manuscript is accepted if required according to the journal that you are submitting your paper to)

[*]Corresponding author. E-mail: yu@physics.ucdavis.edu.

ABSTRACT: Single crystalline vanadium dioxide (VO_2) nanobeams offer an ideal material basis for exploring the widely observed insulator-metal transition in strongly correlated materials. Here we investigate non-equilibrium carrier dynamics and electronic structure in single crystalline VO_2 nanobeam devices using scanning photocurrent microscopy in the vicinity of their phase transition. We extracted a Schottky barrier height of ~0.3 eV between the metal and insulator phases of VO_2, providing direct evidence of the nearly symmetric bandgap opening upon the phase transition. We also observed unusually long photocurrent decay lengths in the insulator phase, indicating unexpectedly long minority carrier lifetimes on the order of microseconds, consistent with the nature of carrier recombination

between two d-subbands of VO_2.

PACS numbers: 71.30.+h, 72.20.Jv, 73.30.+y

Vanadium dioxide (VO_2) is one of the most studied strongly correlated materials. VO_2 undergoes a first-order insulator-metal transition (IMT) at T_c = 68 °C,[1] which involves a drastic change both in electrical resistivity and crystal structure. In its insulating (I) phase ($T < T_c$), VO_2 has a monoclinic crystal structure with a bandgap of ~0.6 eV,[2] which transforms into a tetragonal structure in its metallic (M) phase at higher temperatures ($T > T_c$) (Fig. 1(a)). The electronic structure at the junction of M-I domain walls in VO_2 is of great interest to understanding the mechanism of IMT, but has rarely been directly explored. Intriguing questions remain unanswered such as how the bands line up between the two phases, whether the interface is Ohmic or Schottky, and how much the bands bend at the interface. The answers to these questions can shed light on the IMT mechanism in strongly correlated materials, which is still under debate in the case of VO_2 after decades of studies.[3, 4] In addition, the charge carrier diffusion lengths have not yet been measured in VO_2. Combined with mobilities measured by Hall or field effect, charge carrier lifetimes can be extracted from the diffusion lengths to elucidate the charge carrier dynamics. The difficulties of measuring charge carrier lifetimes in VO_2 are partly due to its inability for light emission, which prevents time-resolved luminescence studies, and unintentional phase transition during pump-probe measurements. Random M-I domain structures that typically occur in VO_2 thin films or bulk specimens also complicate spatially-resolved electrical measurements.[5] Recently, single crystalline VO_2 nanobeams (NBs) with a rectangular cross section have been successfully synthesized via a vapor transport approach.[6] These VO_2 NBs provide an excellent platform for investigating the electronic structure at the M-I junction (domain wall), as the characteristic domain size is larger than the lateral dimension of the NB, so that a simple 1D domain structure can be easily stabilized along the axial direction of the NB.

Scanning photocurrent microscopy (SPCM) is an ideal technique for extracting a number of physical

properties from quasi-1D structures, including electrical field distribution, local band bending, barrier heights, and carrier diffusion lengths.[7-13] A typical SPCM experiment involves rastering a diffraction limited laser spot over a planar device while recording the photocurrent as a function of the local carrier injection position. Spatially resolved photocurrents in VO_2 NBs have been measured previously,[14] but only at very high laser intensity (on the order of 250 kW/cm^2), where the photocurrent is dominated by the thermoelectric effect. In this work, we use laser intensities 1000 times weaker than the previous report, in order to probe intrinsic carrier dynamics by ensuring that the photo-injection does not induce unintentional phase transitions and significant temperature gradients. At this low intensity, the local temperature rise due to laser heating is estimated to be on the order of a Kelvin and we conclude as seen below that the thermoelectric effect can be ignored. We found that the energy band in the n-type I phase bends upward towards the M phase with a barrier height of about 0.3 eV. More interestingly, we observed unexpectedly long minority carrier (hole) diffusion lengths in I phase, indicating long carrier lifetimes on the order of microseconds.

The VO_2 NBs were grown by a physical vapor deposition (PVD) approach in a horizontal tube furnace as detailed in reference 6. Devices incorporating single VO_2 NBs were fabricated by photolithography on the as-grown substrates, where the NBs were partially embedded in the 1.1 μm thick SiO_2 layer on Si wafers. Cr/Au contacts were thermally evaporated, creating 20 μm-gap devices with NBs that typically had a rectangular 1 μm^2 cross-section. SEM image of a typical device is shown in Fig. 2(b). The VO_2 NB devices showed linear current-voltage (I-V) characteristics with contact resistance much lower than the NB resistance, confirmed by 4-probe measurements. The I phase VO_2 NBs were n-type with a relatively low electrical resistivity of ~ 5 Ω·cm. The Kelvin probe microscopy showed that the electric potential was uniformly distributed along a typical NB at room temperature (Fig. 1(b)), indicating the NBs were free of defects that might induce local electric field. The slight nonlinear evolution of voltage profile near the contacts is likely due to the Schottky barriers between the VO_2 NB and the metal electrodes. The spatial resolution of our KPM is on the order of 100 nm, longer

than the expected depletion width, and thus cannot provide a direct measure of this width. As the temperature increased and M domains formed in the NBs, the device resistance decreased in discrete steps. A typical resistance-temperature (R-T) curve can be seen in Fig. 1(c). The temperature dependent conductance of a typical NB device followed the Arrhenius behavior very well with an activation energy of 80 meV (Fig. 1(d)), much smaller than the bandgap, indicating the NBs were highly doped.

Our SPCM setup was based on an Olympus 51× microscope, where a laser beam (CW 532 nm, Compass 315M) was focused by a 100× N.A. 0.95 objective to a Gaussian profile with a full width at half maximum (FWHM) of 900 nm. Great care was taken to ensure that the laser intensity was well below the phase transition threshold, which is about 20 kW/cm^2 at room temperature. Thanks to the drastic difference in reflectivity, M domains can be visualized from optical images.[15] During laser scanning, we constantly checked the NBs optically to ensure no changes in domain configuration occurred. If our laser intensity was above the threshold, we indeed observed the creation of an M domain at the injection position and the M domain moved following the laser spot during the scanning.

We first present the SPCM results of a typical single VO_2 NB device (**D1**) at room temperature (Fig. 2), far from the phase transition temperature (68 °C). The excitation laser peak intensity was 540 W/cm^2, much lower than the phase transition threshold and thus the NB was completely in the I phase during the scanning. A typical SPCM image at zero bias is shown in Fig. 2(b), displaying significant photocurrent only when the illumination is near the contacts. The Schottky junction at the Cr contact leads to zero-bias photocurrent[11] and the current direction indicates an upward band bending towards the electrodes. In the more than 10 devices measured to date, the bending directions have been consistent and agree with the n-type nature of VO_2. An external quantum efficiency (EQE, ratio of collected carriers to incident photons) of 0.006% is estimated from the maximum zero-bias photocurrent (~100 pA) and the excitation intensity (540 W/cm^2). In addition, the current decays exponentially as the laser spot moves away from the contact, with a characteristic length of ~3 μm (Fig. 2(c)).

The photocurrent generated by local excitation in the I phase is unlikely caused by the thermoelectric

current for the following reasons. (1) When the laser spot is near the contact, only a small temperature rise on the order of 0.01 K is estimated at the VO_2/Au thermocouple junction, because of the high thermal conductivity of Au. Such a small temperature difference leads to ignorable thermoelectric current. (2) When the laser spot is near the center of the NB, the expected temperature increase is on the order of 1 K at the local illumination position. At the first glance, this temperature rise seems to lead to a thermoelectric current high enough to account for the measured current level, considering a large Seebeck coefficient of the I phase of 0.4 mV/K.[16] However, the temperature at the left and right Au contacts remains at room temperature. The thermoelectric potential difference between the laser spot and left contact is opposite to that between the laser spot and the right contact. Thus, the thermoelectric current flowing toward the left hand side of the laser spot largely cancels with thermoelectric current flowing toward the right hand side, leading to a small net thermoelectric current. A numerically simulation indeed shows that the thermoelectric current is much smaller than the measured current and can be ignored (J_{TE} in Fig. 3(b)).

The photocurrent decay may also be attributed to the decay in drift current driven by the built-in field in the depletion region at the weak Schottky contacts. However, the depletion region is expected to be $<$ 100 nm in the I phase, considering a dielectric constant of 24 and a high electron density of ~ 10^{18} cm^{-3}.[4, 17] Thus the built-in field in the depletion region is unable to cause the long spatial extension of the photocurrent spots. As recently shown in a thorough modeling of SPCM,[18] carrier diffusion in conjunction with a weak Schottky field can cause a SPCM decay length much longer than the depletion width. Photo-generated carriers can diffuse to the depletion region, be separated by the built-in field at that location, and then be collected by the electrodes. The photocurrent decreases exponentially with the distance x away from the junction ($I = I_0 \exp(-x/L_D)$), as a longer distance results in a smaller fraction of carriers diffusing to the junction and being collected. The excellent exponential fits of our photocurrent data support the validity of this diffusion mechanism. In fact, SPCM is widely regarded as a powerful tool for determining the minority carrier diffusion length.[8, 12, 13] Following the Einstein

relationship, the photocurrent decay length of $L_D = \sqrt{D_p \tau_p}$ = 3.3 μm corresponds to a product of hole mobility (μ_p) and lifetime (τ_p) of $\mu_p \tau_p$ = 4.2 × 10^{-6} cm^2/V. The mobility of the majority carriers (electrons) in n-type VO_2 NBs has been reported to be in the range of 0.1-1.0 cm^2/Vs in the insulator phase.[19] The minority carriers (holes) in the valence band are expected to have comparable or lower mobilities. If taking an upper bound of μ_p = 1 cm^2/Vs for the I phase, a hole lifetime of τ_p ~ 4 μs is expected for free holes. A lower μ_p will yield an even longer lifetime. The rise/fall time of the photocurrent was measured to be 15 μs as the illumination was turned on/off (Fig. S1).[20] This measured response time was limited by the instrumental temporal resolution. Thus we conclude that the hole lifetime is τ_p = 4 − 15 μs.

When a bias up to 200 mV is applied to the NB, the photocurrent is suppressed (enhanced) at the anode (cathode) (Fig. 2(d)), because the external electric field at the anode (cathode) is against (along with) the Schottky field. Besides this photocurrent change at the contacts, the most apparent change of the photocurrent profile under bias is an additional broad peak with higher magnitude appearing around the center of the NB. Note that the dark current is already subtracted in Fig. 2(d). All devices measured to date show the same trend. On the other hand, the photocurrent spots in PbS nanowires[12] and Ge nanowires[21] are always close to one of the contacts under bias. This photocurrent under bias is another indication that the minority carrier lifetime is exceptionally long in VO_2 as shown by comparison with simulations. Following the method described in reference [22], we performed a numerical simulation of the electrodynamics of free carriers in 1D NBs under steady-state local illumination. The parameters used for the simulation are summarized in Table I. The non-equilibrium electrons and holes are generated solely in the illumination area, while they recombine throughout the entire NB.

The simulation shows that for a given 1D system with zero or low energy barriers at the electrodes, weak local illumination typically generates non-equilibrium carriers ($\Delta n = \Delta p$) at much lower densities than the equilibrium majority carrier density ($n_0 = N_d$) coming from intentional or unintentional doping

(Fig. S2(b)).[20] In this "low-level" injection, the photocurrent is very weak and has a flat line shape, with no discernible peak, as shown in Fig. 3(d). This is because the non-equilibrium carriers cannot reach the electrodes unless the laser injection spot approaches one of the electrodes. However, when the minority carrier lifetime (τ_p) is μs long, even a weak illumination could generate non-equilibrium carrier densities much higher than in equilibrium, $\Delta n = \Delta p >> n_0$, thus becoming effectively "high-level" injection (Fig. S2(a)).[20] This is because the recombination rate is low enough to allow a high density of non-equilibrium carriers to accumulate in the steady state. At high-level injection, the photocurrent develops a broad peak under bias, and the peak is located where the total current switches from being limited by electron current (electrons reaching the anode) to being limited by hole current (holes reaching the cathode).[8] When the mobility and lifetime of electrons are comparable to those of the holes, the photocurrent peak is located near the center of the NB, which is the case of the VO_2 NBs. Fig. 3(a) shows the simulated photocurrent profile in this case, which agrees very well with the experimental data (Fig. 2(d)). Also plotted in Fig.s 3(b) and (c) are band bending and current components when the laser is focused near the SPCM peak position in Fig. 3(a).

The long minority carrier lifetime indicates a slow electron-hole recombination. This is consistent with the nature of the electronic bands involved in the recombination. In tetrahedrally bonded, direct-bandgap semiconductors (such as GaAs), the bottom of the conduction band is derived from the atomic s orbital and the top of the valence band is derived from the atomic p orbital, such that electron-hole recombination can readily occur via an s-p dipole transition. In I phase VO_2, on the contrary, both the valence and conduction subbands are split from the same atomic orbital, the vanadium $d_{//}$ ($d_{x^2-y^2}$) band, as shown schematically in Fig. 1(a). The first-order dipole transition is thus forbidden and the radiative recombination rate is thus much slower, resulting in a long minority carrier lifetime governed by non-radiative recombination mediated by defects. Further theoretical and experimental work is required to confirm this conjecture.

In order to study the local band structure associated with the M-I domain walls, SPCM measurements

were performed with M domains present in a NB device (**D2**) at elevated temperatures (Fig. 4). As the temperature was ramped up, the first M domain typically appeared at 55 °C. Multiple M domains nucleated and grew as the temperature was further increased. All M domains eventually merged together, forming a purely M phase NB at a temperature above 100 °C. This domain behavior was explained by substrate-imposed strain effects.[23] Different domain configurations were obtained and stabilized by carefully controlling the NB temperature. Excitation intensity was further reduced to avoid unintentional transitions and the NBs were monitored optically to ensure that the domain configuration remained the same during the laser scanning. The weak illumination intensity is expected to raise the temperature by approximately 0.2 K locally. The M domain has a much lower Seebeck coefficient than that of the I phase, but the M domain is short and the temperature difference across it is ignorable. Therefore, the thermoelectric current toward the right and the left contacts should still largely cancel each other as discussed earlier and can be ignored.

The SPCM results obtained with one and two M domains are shown in Fig. 4(a) and (b), respectively. Photocurrent spots of opposite polarity were seen on each side of an M domain and the signs of the photocurrent spots were independent of the size and the number of M domains. The photocurrent signs are consistent with an upward band bending toward the M domain (band diagrams shown in Fig. 4). But the linear I-V curve and the reduced resistance with M domains present suggest that the contact resistance at M-I interface is still low compared with the I phase resistance. To our knowledge, this is the first report on the band bending at the M-I domain wall in VO_2. The band bending direction suggests the initial Fermi level of the M phase lies below the Fermi level of the I phase, which is close to the bottom of the conduction band as the I phase is unintentionally highly n-doped.[17] Since both phases of VO_2 are not piezoelectric, strain at the domain wall is not expected to induce an electric field. In addition, the photocurrent also decays exponentially in the I phase at 55 °C, consistent with the room temperature measurements (Fig. 4(a)). The decay length of 2.2 μm (line plot and fitting not shown) is slightly shorter than the 3.1-3.5 μm at room temperature in the same device, presumably because of a

shorter carrier lifetime at higher temperatures.

In order to extract the barrier height, we model the VO_2 NB device by an equivalent circuit, treating the M-I interface as a Schottky diode. Each M domain is associated with two Schottky barriers, equivalent to two diodes connected back to back. Assuming ideal contacts and identical barrier height at each side of the M domain, the single M domain configuration with the excitation on the left domain wall can be modeled by the circuit diagram in Fig. 4(a). The current obeys the following equation:

$$-\frac{kT}{|e|}\ln\left(\frac{I}{I_0}+1\right)+\frac{kT}{|e|}\ln\left(\frac{I_L-I}{I_0}+1\right)+V_b-IR=0 \quad (1)$$

where I_L is the current generated by light, I_0 is the saturation current of an individual diode, V_b is the bias voltage, R is the total NB I phase resistance, k is the Boltzmann constant, T is the temperature, and $|e|$ is the electron charge. If the current is small ($I << I_0$ and $I_L - I << I_0$), Equation (1) can be simplified to:

$$I=\frac{V_b+kTI_L/|e|I_0}{R} \quad (2)$$

Equation (2) predicts a linear relation between I and V_b, consistent with the linear I-V curves measured under local excitation. Taking the experimental values of the short-circuit current I_{sc} = 60 pA and R = 1 MΩ, we obtain I_L/I_0 = 0.0023, which confirms the small current assumption since $I < I_L << I_0$. Assuming a 100% internal charge separation efficiency η_{cc} (defined by the fraction of the light generated carrier flux to the absorbed photon flux: $\eta_{cc} = I_L/qF$), we obtained I_0 = 0.5 mA. We can then estimate the barrier height ϕ assuming that the current is dominated by thermionic emission:

$$J_0=A^*T^2e^{-\phi/kT} \quad (3)$$

where A* is the Richardson constant (proportional to electron effective mass m_e* = 60 m_0 in VO_2[24]) and J_0 is the saturation current density (= I_0 / area). By using the I_0 value obtained from the circuit model, the barrier was calculated to be approximately $\phi = 0.28$ eV. We note that this value depends on the η_{cc} logarithmically and is the lower boundary of the actual barrier height. A charge separation efficiency η_{cc}

= 100% is indeed expected as the charge transit time across the injection area is much shorter than the carrier lifetime.[25] Even if η_{cc} = 10% instead of 100%, this only increases the calculated barrier height slightly to $\phi = 0.31$ eV as the dependence is logarithmic.

The barrier height at the M-I junction is a direct measure of the band offset between the M and I phases, which is useful for understanding the IMT and has not yet been obtained experimentally. The measured ~ 0.3 eV barrier height provides direct evidence that the Fermi level of the M phase is near the middle of the bandgap ($E_g \sim 0.6 - 0.7$eV) of the I phase in VO_2. As shown by the schematic band diagram in Fig. 1(a), this indicates a nearly symmetric opening of the $d_{//}$ band into the bandgap when the M phase transitions to the I phase. This is consistent with the picture of Mott transition, where the narrow d-band is symmetrically split into the upper and lower Hubbard subbands. This also indicates that the upward shift of the d_π band is important, such that its bottom is not much lower than that of the $d_{//}$* band (Fig. 1(a)).

The direct identification of a Schottky junction at the M-I domain wall also indicates a space charge region between the coexisting I and M phases. As the band in the I phase bends at the M-I junction, the charge density is greatly reduced in the associated depletion region. In the Mott transition picture, thermal activation increases the charge density (n) to a threshold value and triggers the transition and the consequent crystal structure change.[17, 26] Thus, the depletion region at the M-I domain wall effectively presents an energy barrier to the IMT, because additional electrons need to be injected into the depletion region to meet the charge density threshold in order for the M domain to expand.

In summary, we have studied the insulator-metal transition in VO_2 nanobeams by scanning photocurrent microscopy. We observed a band bending arising from the Schottky junction at the M-I domain wall. The barrier height extracted from the photocurrent indicates that the Fermi level of the M phase lies near the middle of the I phase bandgap, suggesting a symmetric bandgap opening upon the phase transition. We also observed unexpectedly long minority carrier diffusion lengths in the I phase. We attribute the photocurrent to carrier diffusion and extract a long recombination lifetime on the order

of μs from the SPCM data, which is consistent with a slow carrier recombination across the d-subbands of VO_2.

Acknowledgement. The SPCM characterization was supported by the U.C. Davis Startup fund and the Hellman fellowship. Materials synthesis (J.W.) was supported by an NSF CAREER Award under grant number DMR-1055938. Modeling (D. F.) was supported by the Graduate Student Research Innovation Project of Jiangsu Province of China (Grant No. CX09B_009Z).

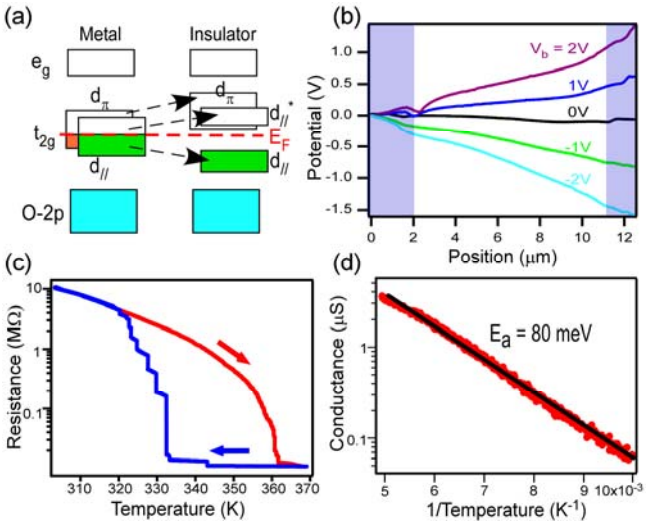

FIG. 1. (Color online) (a) Band diagram for M and I phases of VO_2, showing the splitting of the $d_{//}$ band and the rising of the d_π band upon transition from the tetragonal (M) to monoclinic (I) crystal structures. (b) Kelvin probe microscopy measurement of a VO_2 NB at room temperature. Shaded areas indicate electrodes. (c) Resistance as a function of temperature for a typical VO_2 NB device (device **D1**). The arrows indicate the temperature ramping directions. (d) Conductance as a function of inverse temperature showing an activation energy of 80 meV.

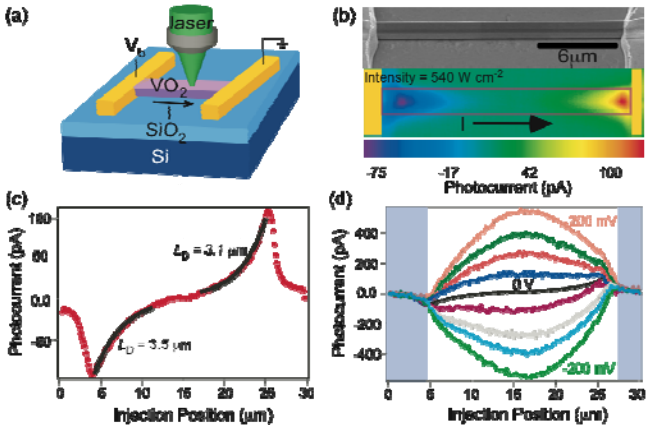

FIG. 2. (Color online) (a) Schematic of SPCM setup, where a diffraction limited laser spot is rastered over a VO_2 NB device. (b) SEM image and SPCM image of a VO_2 NB at zero-bias with illumination intensity of 540 W cm^{-2} and wavelength of 532 nm (device **D1**). The arrow indicates the positive current direction. (c) Cross section of the SPCM image in (b) along the axial direction of the NB. The data is fit to the exponential form $I = I_0 \exp[-(x - x_0)/L_D]$. The fitting parameters L_D are labeled in the plot. (d) SPCM line scans under biases ranging from −200 mV to 200 mV with 50 mV increments. The dark current was subtracted.

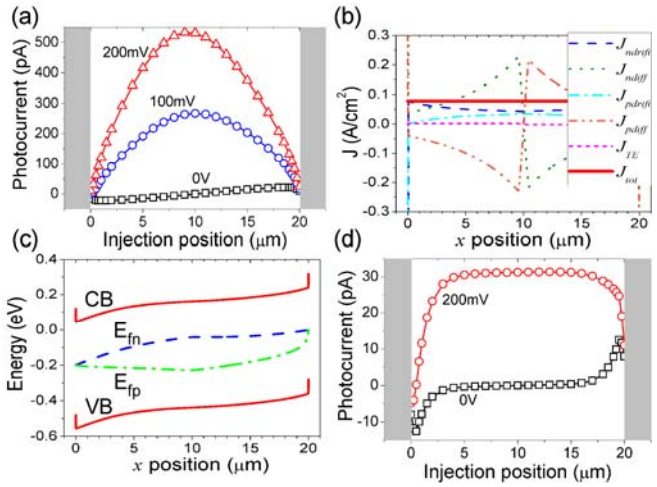

FIG. 3. (Color online) (a) Numerically simulated photocurrent of a VO_2 NB using the parameters summarized in Table I Scenario A. Bias voltage is 0, 100mV and 200 mV, respectively, as labeled. The dark current was subtracted. (b) Simulated steady-state density of total current and current components when the laser is focused at 10 μm. J_{ndrift}, J_{ndiff}, J_{pdrift}, J_{pdiff}, J_{TE} and J_{tot} are electron drift current, electron diffusion current, hole drift current, hole diffusion current, thermoelectric current and total current, respectively. (c) Band diagram corresponding to (b). CB, VB, E_{fn} and E_{fp} are conduction band minimum, valence band maximum, electron quasi Fermi level and hole quasi Femi level, respectively. (d) Numerically simulated photocurrent of a VO_2 NB using the parameters summarized in Table I Scenario B (shorter lifetimes). Bias voltage is 0 and 200 mV, respectively, as labeled.

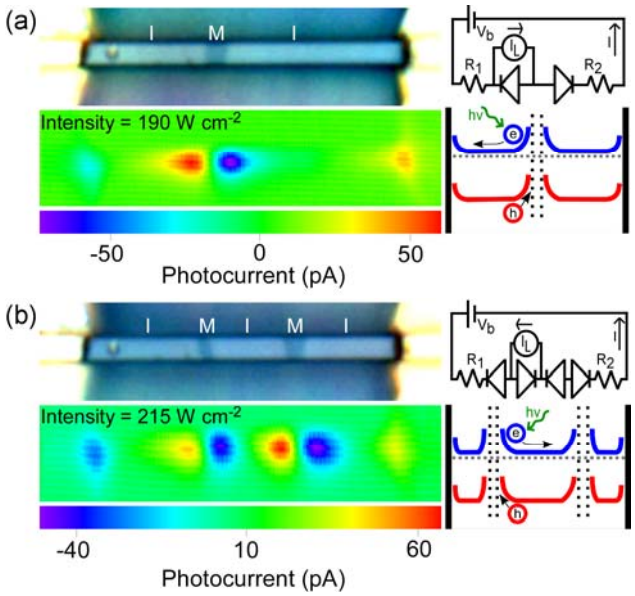

FIG. 4. (Color online) (a) Optical image and zero-bias SPCM image of a VO_2 NB with a single M domain at 55 °C (Device **D2**). Circuit model and band diagram are shown on the right. (b) The same device with two separate M domains at slightly higher temperature. Note the positive direction of the current is defined from left to right for both cases.

TABLE I. Physical parameters used in the numerical simulation in FIG. 3.

Scenario	Bandgap (eV)	N-type doping $(cm^3)^{17}$	Mobility (cm^2/Vs) ^{19}	Lifetime (μs)	Effective mass $(m_0)^4$	Laser wavelength (nm)	Laser intensity (W/cm^2)	Barrier height (eV)
A	0.6	10^{18}	μ_n=0.5 μ_p=0.5	τ_n=10 τ_p=10	m_n=60 m_p=60	532	540	0.32
B	0.6	10^{18}	μ_n=0.5 μ_p=0.5	τ_n=0.5 τ_p=0.5	m_n=60 m_p=60	532	540	0.32

References and Notes

1 F. J. Morin, Phys. Rev. Lett. **3**, 34 (1959).

2 H. W. Verleur, A. S. Barker, and C. N. Berglund, Phys. Rev. **172**, 788 (1968).

3 N. F. Mott, Rev. Mod. Phys. **40**, 677 (1968).

4 P. P. Edwards, R. L. Johnston, C. N. R. Rao, D. P. Tunstall, F. Hensel, Philos. Trans. R. Soc. London, Ser. A **356**, 5 (1998).

5 M. M. Qazilbash, M. Brehm, B.-G. Chae, P. C. Ho, G. O. Andreev, B.-J. Kim, S. J. Yun, A. V. Balatsky, M. B. Maple, F. Keilmann, H.-T. Kim, D. N. Basov, Science **318**, 1750 (2007).

6 B. S. Guiton, Q. Gu, A. L. Prieto, M. S. Gudiksen, H. Park, J. Am. Chem. Soc. **127**, 498 (2004).

7 Y. Ahn, J. Dunning, and J. Park, Nano Lett. **5**, 1367 (2005).

8 Y. Gu, J. P. Romankiewicz, J. K. David, J. L. Lensch, L. J. Lauhon, Nano Lett. **6**, 948 (2006).

9 Y. H. Ahn, A. W. Tsen, B. Kim, Y. W. Park, J. Park, Nano Lett. **7**, 3320 (2007).

10 Y.-J. Doh, K. N. Maher, L. Ouyang, C. L. Yu, H. Park, Nano Lett. **8**, 4552 (2008).

11 J. E. Allen, E. R. Hemesath, and L. J. Lauhon, Nano Lett. **9**, 1903 (2009).

12 R. Graham, C. Miller, E. Oh, D. Yu, Nano Lett. **11**, 717 (2011).

13 M. C. Putnam, D. B. Turner-Evans, M. D. Kelzenberg, S. W. Boettcher, N. S. Lewis, H. A. Atwater, Appl. Phys. Lett. **95**, 163116 (2009).

14 B. Varghese, R. Tamang, E. S. Tok, S. G. Mhaisalkar, C. H. Sow, J. Phys. Chem. C **114**, 15149 (2010).

15 A. Tselev, E. Strelcov, I. A. Luk'yanchuk, J. D. Budai, J. Z. Tischler, I. N. Ivanov, K. Jones, R. Proksch, S. V. Kalinin, A. Kolmakov, Nano Lett. **10**, 2003 (2010).

16 J. Cao, W. Fan, H. Zheng, J. Wu, Nano Lett. **9**, 4001 (2009).

17 J. Cao, W. Fan, K. Chen, N. Tamura, M. Kunz, V. Eyert, J. Wu, Phys. Rev. B **82**, 241101 (2010).

18 D. Fu, J. Zou, K. Wang, R. Zhang, D. Yu, J. Wu, Nano Lett. **11**, 3809 (2011).

19 C. N. Berglund and H. J. Guggenheim, Phys. Rev. **185**, 1022 (1969).

20 See Supplemental Material at [URL will be inserted by publisher] for a temporal photo-response measurement and more simulation results.

21 C.-J. Kim, H.-S. Lee, Y.-J. Cho, K. Kang, M.-H. Jo, Nano Letters **10**, 2043.

22 M. Rini, Z. Hao, R. W. Schoenlein, C. Giannetti, F. Parmigiani, S. Fourmaux, J. C. Kieffer, A. Fujimori, M. Onoda, S. Wall, A. Cavalleri, Applied Physics Letters **92**, 181904 (2008).

23 J. Wu, Q. Gu, B. S. Guiton, N. P. de Leon, L. Ouyang, H. Park, Nano Lett. **6**, 2313 (2006).

24 A. Zylbersztejn and N. F. Mott, Phys. Rev. B **11**, 4383 (1975).

25 η_{cc} is determined by the carrier recombination rate k_r and the charge separation rate k_{cc} ($\eta_{cc} = \frac{k_{cc}}{k_{cc} + k_r}$). The carrier recombination rate k_r can be estimated from the inverse of the carrier lifetime ~10^5 s^{-1} and the charge separation rate can be estimated from the inverse of the charge transit time $k_{cc} = \frac{D_p}{w^2}$ = 10^6 s^{-1}, where we take the laser beam width w = 1 μm and the diffusion coefficient D_p = 0.01 cm^2/s for μ_p = 0.5 cm^2/Vs.

26 N. F. Mott, *Metal–Insulator Transitions* (Taylor & Francis, 1990).